Soft Matter

PAPER

View Article Online
View Journal | View Issue



Cite this: *Soft Matter*, 2021, **17**, 6470

# Self-assembly of stimuli-responsive coiled-coil fibrous hydrogels†

Michael Meleties, ‡[a] Priya Katyal, ‡[a] Bonnie Lin, [a] Dustin Britton [a] and Jin Kim Montclare *[abcd]

Received 26th May 2021,
Accepted 11th June 2021

DOI: 10.1039/d1sm00780g

rsc.li/soft-matter-journal

Owing to their tunable properties, hydrogels comprised of stimuli-sensitive polymers are one of the most appealing scaffolds with applications in tissue engineering, drug delivery and other biomedical fields. We previously reported a thermoresponsive hydrogel formed using a coiled-coil protein, Q. Here, we expand our studies to identify the gelation of Q protein at distinct pH conditions, creating a protein hydrogel system that is sensitive to temperature and pH. Through secondary structure analysis, transmission electron microscopy, and rheology, we observed that Q self-assembles and forms fiber-based hydrogels exhibiting upper critical solution temperature behavior with increased elastic properties at pH 7.4 and pH 10. At pH 6, however, Q forms polydisperse nanoparticles, which do not further self-assemble and undergo gelation. The high net positive charge of Q at pH 6 creates significant electrostatic repulsion, preventing its gelation. This study will potentially guide the development of novel scaffolds and functional biomaterials that are sensitive towards biologically relevant stimuli.



## Introduction

The field of biomaterials is embracing peptides and proteins as building blocks that self-assemble into nanostructures such as nanoparticles or nanofibers.[1–4] Hierarchical self-assembly of these nanoarchitectures enables the formation of supramolecular hydrogels.[5] Proteins that undergo gelation in response to external stimuli have found numerous applications in the bioengineering and biomedical fields.[6,7] To generate such smart biomaterials, there is an increasing trend to develop systems that can respond to a multitude of stimuli.[8] Although thermosensitive hydrogels are one of the widely studied and well-understood class of protein biomaterials, substantial progress is also reportedly being made in incorporating stimuli-responsiveness to pH, light, ionic strength, redox, as well as the addition of small molecules.[9–12]

While a wealth of literature is dedicated towards beta-rich fibrils and gels,[13–16] fibrous hydrogels made up of coiled-coil proteins also exhibit tunable gelation, stemming from the oligomerization of coiled-coils acting as physical cross-links.[13,17] One such example includes the triblock protein reported by Petka *et al.*, which is comprised of two terminal leucine zippers connected *via* a central alanine–glycine rich polyelectrolyte block.[18] These hydrogels have been shown to undergo a gel-to-solution (gel–sol) transition in response to increasing pH and temperature due to the dissociation of coiled-coil oligomers making up the three-dimensional matrix.[18] A relatively simpler design based on a single α-helical peptide has been described by Fletcher *et al.*[9] AFD19, a 21-residue long peptide, forms a gel at pH 6. A charge of +1 and −1 is suitable for maintaining fibril solubility and promoting fibril–fibril associations to form a physically cross-linked hydrogel.[9] A single site mutation of AFD19 results in AFD36, which forms a coiled-coil-based hydrogel at physiological pH and salt conditions.[19] These gels can support the growth of mouse fibroblasts and have potential in tissue engineering applications.[19]

A two-component system based on self-assembling fibers (SAFs) has also been utilized for supporting cell growth and differentiation.[20] The hydrogels are formed upon mixing equimolar amounts of complementary SAF peptides and incubating on ice for 30 min or 5 min on ice followed by incubation at 20 °C for 25 min. Since these low-temperature gels are not stable for long-term cell culture studies, a new SAF combination has been designed that exhibits gelation at room temperature and remains stable at 37 °C for a period of two weeks.[20] Recently, we have reported a low temperature protein hydrogel that is capable of encapsulating and releasing small hydrophobic molecules over 17–18 days at 37 °C.[21] The hydrogel is based on a single coiled-coil protein Q (Table S1, ESI†), which is derived from the coiled-coil domain of cartilage oligomeric

[a] *Department of Chemical and Biomolecular Engineering, New York University Tandon School of Engineering, Brooklyn, New York, 11201, USA. E-mail: montclare@nyu.edu*
[b] *Department of Radiology, New York University Langone Health, New York, New York, 10016, USA*
[c] *Department of Biomaterials, New York University College of Dentistry, New York, New York, 10010, USA*
[d] *Department of Chemistry, New York University, New York, New York, 10003, USA*
† Electronic supplementary information (ESI) available. See DOI: 10.1039/d1sm00780g
‡ M. M. and P. K. contributed equally to this work.

matrix protein (COMPcc).[22] Q self-assembles to form nanofibers and undergoes physical entanglement to form hydrogels at low temperatures, exhibiting upper critical solution temperature (UCST) phase behavior.[21] Since the overall charge of the protein, governed by external pH conditions, can influence its UCST phase transition,[23] we explore the role of pH on the self-assembly of Q. Here, we investigate the gel formation of Q protein at distinct pH conditions, creating a protein hydrogel system that is sensitive to temperature and pH.

In this study, the behavior of Q at pH 6, 7.4, and 10 is characterized with the aim of understanding how the differing pH and charge affects fiber assembly and subsequent gelation. Specifically, effects of pH on secondary structure, fiber assembly, and rheological properties are explored. Our studies demonstrate that pH is one of the factors that governs the self-assembly of Q. Increasing the pH yields stronger fiber networks, which results in hydrogels with faster gelation times and increased elasticity. The ability of Q to self-assemble into fibers is further established as necessary for gelation to occur, as particle formation at pH 6 prevents higher-order assembly of Q. The significance of this work lies in the further development of novel biomaterials as well as the development of a method to screen key gelation properties in a high-throughput manner.

## Materials & methods

### Materials

M15MA *Escherichia coli* cells[24] were a gift from David Tirrell (California Institute of Technology). Tryptic soy agar, ampicillin, kanamycin, sodium phosphate monobasic monohydrate ($NaH_2PO_4 \cdot H_2O$), sodium phosphate dibasic anhydrous ($Na_2HPO_4$), ammonium chloride ($NH_4Cl$), potassium phosphate monobasic ($KH_2PO_4$), sodium hydroxide (NaOH), dextrose monohydrate (D-glucose), magnesium sulfate ($MgSO_4$), calcium chloride ($CaCl_2$), isopropyl β-D-1-thiogalactopyranoside (IPTG), tris–hydrochloride (Tris–HCl), pierce bicinchoninic acid (BCA) assay kit, pierce snakeskin dialysis tubing 3.5 kDa molecular weight cut off (MWCO), sodium dodecyl sulfate (SDS) were acquired from Thermo Fisher Scientific. Imidazole was purchased from Acros Organics. HiTrap immobilized metal affinity chromatography (IMAC) fast flow (FF) 5 mL column for protein purification and Whatman filter paper for transmission electron microscopy (TEM) sample preparation were purchased from GE Healthcare Life Sciences. Macrosep and Microsep Advance centrifugal devices 3 kDa MWCO and 0.2 μm syringe filters were purchased from Pall Corporation. Acrylamide/bis-acrylamide solution (30%) 29 : 1 and natural polypeptide sodium dodecyl sulfate–polyacrylamide gel electrophoresis (SDS–PAGE) standard were purchased from Bio-Rad. Formvar/carbon-coated copper grids (FCF400-Cu) and 1% uranyl acetate for TEM were purchased from Electron Microscopy Sciences.

### Expression and purification

Q protein was expressed as described previously.[21] Briefly, the protein was expressed in chemically competent M15MA *Escherichia coli* cells carrying the kanamycin-resistant pREP4 plasmid and induced with IPTG at a final concentration of 200 μg $mL^{-1}$. The cells were harvested and stored at −80 °C until purification. His-tag bearing Q protein was purified using Buffer A (50 mM Tris–HCl, 500 mM NaCl, pH 8) on a HiTrap IMAC FF 5 mL column charged with cobalt(II) chloride. The protein was eluted using a gradient of Buffer B (50 mM Tris–HCl, pH 8, 500 mM NaCl, 500 mM imidazole) with an increasing concentration of imidazole ranging from 10–500 mM. All fractions were assessed *via* 12% SDS–PAGE. The desired fractions were dialyzed using 50 mM Tris–HCl, 500 mM NaCl at pH 6, 7.4 and 10.

### Inversion test

Q protein was concentrated to 2 mM *via* centrifugal filtration. The concentration was determined using BCA assay. The purity of concentrated Q was confirmed using 12% SDS–PAGE. The solution-to-gel phase transition was determined using the tube-inversion method. A 150 μL aliquot of Q at 2 mM (in 50 mM Tris–HCl, 500 mM NaCl) under pH conditions of 6, 7.4 and 10 was incubated at 4 °C in a 2 mL Eppendorf tube and visually inspected by inverting the tubes at different timepoints. Gelation was confirmed when a solid gel-like material was observed that did not flow under its weight.

### Rheology

The rheological properties of Q hydrogels at pH 6, 7.4 and pH 10 were determined using a stress-controlled rheometer (ARES-G2, TA Instruments, New Castle, DE). The rheometer was equipped with 8 mm diameter parallel plates with a 0.2 mm geometry gap. Oscillatory frequency sweeps were used to determine the storage moduli ($G'$) and the loss moduli ($G''$) as a function of frequency over a range of 0.1–10 Hz with an oscillation strain of 5%. Measurements were carried out at 4 °C for each pH.

### Circular dichroism

Circular dichroism (CD) spectroscopy was carried out using a Jasco J-815 CD spectrometer equipped with a PTC-423S single position Peltier temperature control system. A 2 mM solution of Q protein at pH 6, 7.4 and 10 was incubated at 4 °C for 96 h. Q solution at pH 6 and gel samples at pH 7.4 and pH 10 were diluted with deionized water to a final concentration of 10 μM prior to measurement. Operation and analysis parameters were adapted as described previously.[21] Wavelength scans were performed from 250 to 190 nm with a 1 nm step size at 4 °C. Buffer scans were performed at each pH and subtracted from wavelength scans.

### Attenuated total reflectance-Fourier transform infrared (ATR-FTIR) spectroscopy

ATR-FTIR spectroscopy was used to assess the secondary structure of Q. A Nicolet 6700 Fourier Transform Infrared spectrometer equipped with a diamond ATR accessory and a mercury cadmium telluride (MCT-A) detector was used to collect the spectra of the samples. For each sample, 5 μL of Q at a concentration of 2 mM was spotted onto the diamond surface and allowed to dry for 5 minutes. The spectrum was obtained across a range of 4000–400 $cm^{-1}$ with a resolution of 0.5 $cm^{-1}$ at room temperature for a total of 128 scans.

PeakFit software (Version 4.12, Systat Software, Inc.) was utilized for peak deconvolution.[21,25] To determine the secondary structure content, each spectrum was deconvoluted in the amide I region (1600–1700 $cm^{-1}$). Data processing consisted of a second derivative zero baseline correction and using Gaussian functions to fit the spectrum within PeakFit.[26] The number and relative locations of peaks were determined by investigating the second derivative of the processed spectra. Peak deconvolution was then carried out on the processed spectrum, with each deconvoluted peak having a full-width at half-maximum less than 30 $cm^{-1}$, and was complete when the coefficient of determination was $r^2 \geq 0.99$.[26]

### Transmission electron microscopy

FEI Talos L120C transmission electron microscope (TEM) equipped with Gatan 4k × 4k OneView camera was used to study the self-assembly of Q at different pH conditions. Samples were diluted to 50 μM and spotted on Formvar/carbon-coated copper grids. The samples were washed with water and then stained with 5 μL of 1% v/v uranyl acetate solution. The fibers were sized using ImageJ software (Version 1.52q).[27]

### Electrostatic potential modeling

ROSETTA suite of macromolecular modeling tools (Version 3.5) was used to set up a symmetric starting model of Q based on its wild-type derivative, COMPcc, with crystal structure (PDB: 3V2P). PDB2PQR software (Version 3.1.0) was used to setup the titration states at room temperature using the amber[28] forcefield and propka[29,30] pH calculation method. The p$K_a$ values of ionizable residues determined by propka calculations were used in modified Henderson–Hasselbalch equations to calculate the charge of positive and negative residues (eqn (1) and (2), respectively) as functions of pH, which were then summed to determine the net charge of Q as a function of pH and the isoelectric point (pI).[9,31] PDB2PQR subsequently makes an input file that is used for Adaptive Poisson–Boltzmann Solver (APBS) electrostatic software (Version 3.0.0) to calculate the electrostatic potential map of Q as a function of pH.

$$\text{Negative residue charge} = -\frac{10^{(\text{pH}-\text{p}K_a)}}{1+10^{(\text{pH}-\text{p}K_a)}} \quad (1)$$

$$\text{Positive residue charge} = 1-\frac{10^{(\text{pH}-\text{p}K_a)}}{1+10^{(\text{pH}-\text{p}K_a)}} \quad (2)$$

## Results and discussion

Q (Table S1, ESI†) was successfully purified and concentrated at each of the studied pH conditions. The purity at each pH was measured using SDS–PAGE and confirmed to be greater than 99% pure (Fig. S1, ESI†). Its ability to assemble into a hydrogel was screened using a tube-inversion test.[32] The gelation of Q protein was investigated at a pH range of 6–10, with further characterization pursued at pH 6, 7.4 and 10. At pH 6, no gelation was observed for Q over a two-week time period, with Q collapsing under its own weight upon inversion (Fig. 1a). Similar to previous work at pH 8,[21] Q at pH 7.4 was shown to form a hydrogel within 96 h (Fig. 1b). At pH 10, gelation of Q was observed within a 24 h time period (Fig. 1c). At pH 7.4 and pH 10, Q gels exhibit a gel–sol transition at 37 °C. For pH 7.4, the gel transitioned back into solution in 30 min, while for pH 10, the gel–sol transition occurred over a period of 1 h 30 min (Fig. S2, ESI†). The phase behavior was also shown to be reversible, being able to form a hydrogel again after further incubation at 4 °C (Fig. S2, ESI†). An initial screening of gelation was also done for the same pH levels at room temperature (RT). Among the three different pH conditions tested, gelation was observed only for pH 10 at RT within 48 h of incubation.

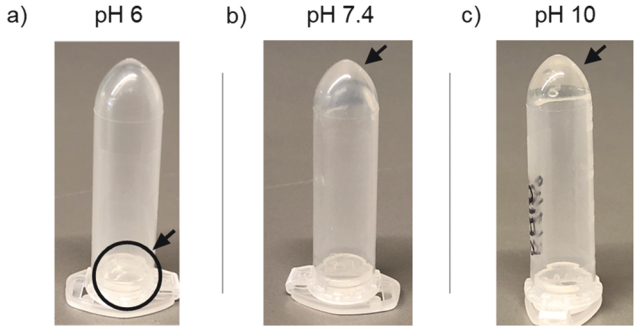


Fig. 1 Tube inversion test of Q at (a) pH 6, (b) 7.4 and (c) 10. Q at pH 6 remains in solution (indicated by arrow) while at pH 7.4 and pH 10, a hydrogel (indicated by respective arrows) is formed in 96 h and within 24 h, respectively, which remains at the bottom of the tube even when inverted.

To assess the effect of pH on secondary structure and associated gelation, CD spectroscopy is carried out. At each pH (6, 7.4 and 10), at a concentration of 10 μM, Q showed the characteristic α-helical signature (Fig. 2). The ratios of the molar residue ellipticities (MRE) at 208 and 222 nm ($\theta_{222}/\theta_{208}$) are used to compare the helical propensity at each pH (Table 1), with an increase in the ratios being observed across the range studied. At pH 6, Q exhibits an intense negative band at 208 nm (Fig. 2a), indicating the presence of isolated α-helices. At pH 10, a $\theta_{222}/\theta_{208}$ ratio of 1.01 is observed, characteristic of increased coiled-coil content under dilute conditions.[33] At pH 7.4, an intermediate ratio of 0.72 is detected. To confirm the secondary structure of Q at each pH at concentrations capable of forming gels, ATR-FTIR is conducted. In evaluating the IR spectra at different pH, the overall spectrum is first inspected for its overall signature. At all pH, a characteristic signature of the pentameric coiled-coil first elucidated by Heimburg *et al.* for COMPcc is observed.[34,35] All spectra reveal a maximum near 1650 $cm^{-1}$, indicating a significant contribution of α-helical content (Fig. 3). Q gel at pH 10 demonstrates a noticeable shoulder peak at 1636 $cm^{-1}$ and a minor peak 1623 $cm^{-1}$, with these peaks shifted to the lower wavelengths as the pH is decreased. At pH 6, the peaks shift to 1629 and 1617 $cm^{-1}$, indicating a lower coiled-coil content, consistent with the CD data. Although these minor peaks overlap with the wavenumbers that are typically assigned to ß-structures,[36] our hydrogels favor α-helical assembly at neutral and higher pH owing to the major peak observed at 1650 $cm^{-1}$. Previous work has demonstrated that the network of interactions that stabilizes coiled-coils are

 

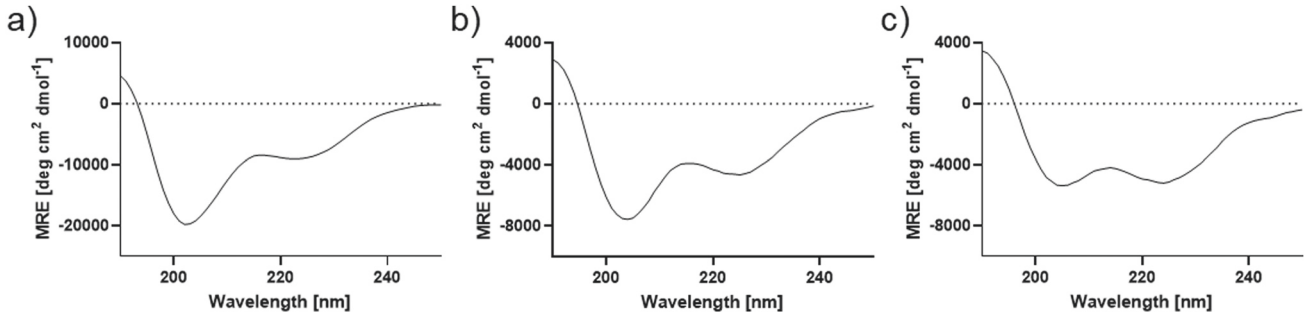


Fig. 2 Molar residue ellipticities of Q at (a) pH 6, (b) pH 7.4, and (c) pH 10 in the far-UV region. Samples were diluted from 2 mM to 10 μM prior to wavelength scans being collected. Spectra shown are averages of three independent trials.

Table 1 Molar residue ellipticities for Q at pH 6, 7.4, and 10 at 208 and 222 nm. Ratios of the MRE at 208 and 222 nm ($\theta_{222}/\theta_{208}$) were used to compare the α-helicity

| pH | $\theta_{222}$ (deg cm$^2$ dmol$^{-1}$) | $\theta_{208}$ (deg cm$^2$ dmol$^{-1}$) | $\theta_{222}/\theta_{208}$ |
|---|---|---|---|
| 6 | −9057.6 | −15091.5 | 0.60 |
| 7.4 | −4541.2 | −6338.4 | 0.72 |
| 10 | −5071.2 | −5044.0 | 1.01 |

sensitive to pH and are abrogated at acidic pH.[37] This is similar to our observations at pH 6, where isolated α-helices are unable to interact to form a gel.

The entangled fiber network formed by Q has been previously shown to be the basis of hydrogel formation.[21] Consistent with the previous studies, TEM reveals the presence of fibers at pH 7.4 and 10, with a more densely cross-linked network observed at pH 10 (Fig. 4). The average size of the fibers at pH 7.4 and pH 10 are 21.8 ± 4.9 and 16.7 ± 3.2, respectively. Whereas at pH 6, nanoparticles (NPs) (Fig. 4a) that cluster together to form large aggregates are observed. Q-NPs are akin to the self-assembling protein nanoparticles (SAPN), particularly arginine-bearing SAPN reported by Indelicato *et al.*[38] However, unlike Q-NPs, SAPNs comprise of two oligomeric domains and assume the icosahedral symmetry.[38] Q-NPs at pH 6 are notably different from the nanoparticles formed by a 34-residue *de novo* peptide that self-assembles to form coiled-coil based fibers at slightly acidic pH but assembles to form NPs at pH 7.[39] Further studies will be required to delineate the mechanism of nanoparticles

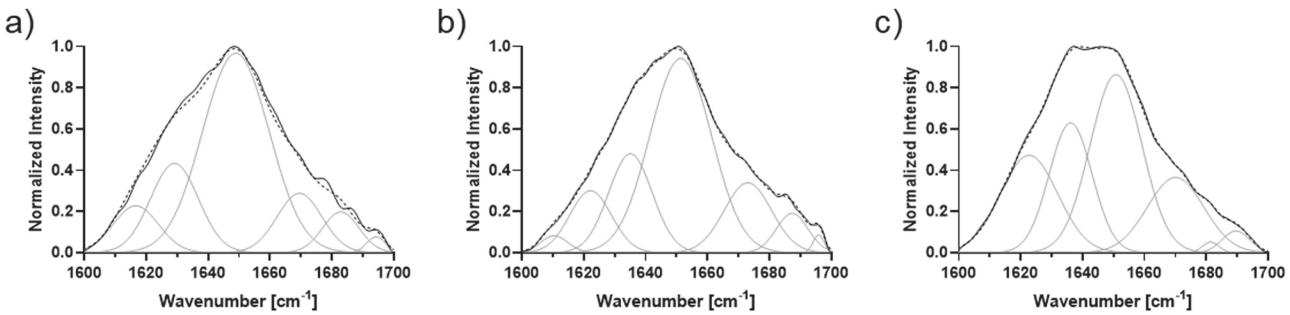


Fig. 3 ATR-FTIR spectral analysis of Q secondary structure as a (a) solution at pH 6 and as a hydrogel at pH (b) 7.4 and (c) 10. Representative spectra at each condition of Q at 2 mM following incubation at 4 °C. Observed spectra are indicated by solid black lines and overall spectra generated by deconvolutions indicated by dashed black lines. Peaks from resulting deconvolution are indicated in gray.

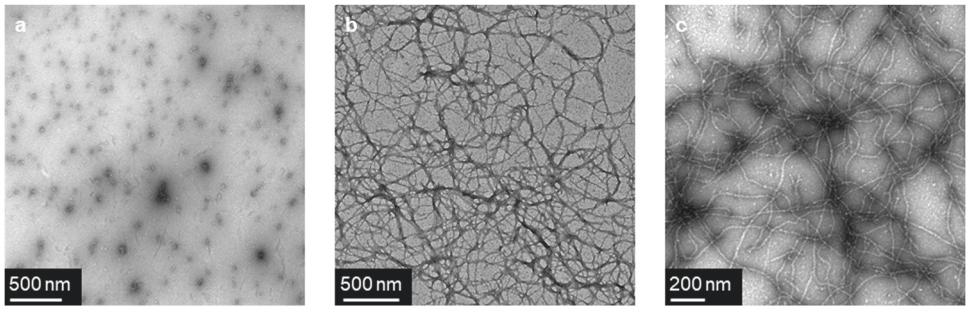


Fig. 4 Nanoassembly of Q shown by TEM as (a) a solution at pH 6 and as a hydrogel at (b) pH 7.4, and (c) pH 10. Scale bars indicated as 500 nm for (a) and (b) and 200 nm for (c).

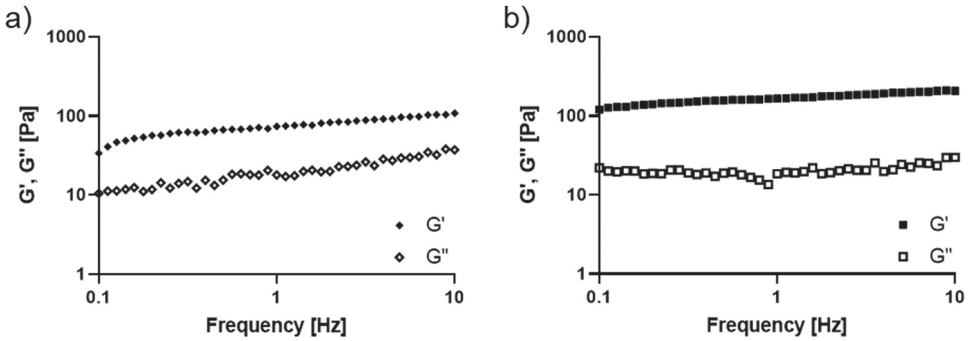


Fig. 5 Rheological properties of Q hydrogel at (a) pH 7.4, and (b) pH 10. Storage ($G'$) (filled) and loss ($G''$) (empty) moduli were determined over a frequency range of 0.1–10 Hz at a constant 5% oscillatory strain at 4 °C. Results shown are the average of two independent trials.

formation; nevertheless the lack of fiber formation at pH 6 impacts the ability of Q to self-assemble into a hydrogel.

To evaluate the rheological properties of Q gels at each pH, a standard parallel plate rheometer is used. For both pH 7.4 and 10, the elastic nature of the Q hydrogels is confirmed, with $G'$ being greater than $G''$ over the range of frequencies studied at 4 °C (Fig. 5). The degree of fibrous entanglement manifests itself in the increased storage moduli ($G'$) of the respective hydrogels, with a higher degree of crosslinking resulting in increased elasticity. The increase of $G'$ to 207.3 Pa for pH 10 compared to 108.9 Pa for pH 7.4 confirms a higher degree of cross-linking in its network at a higher pH compared to pH 7.4. Additionally, examination of the phase angle ($\delta$) can reveal the nature of the material's deformation, with $\tan(\delta)$ ranging from 0 for an ideally elastic behavior to 1 for ideally viscous flow behavior. The phase angle for Q at both pH 7.4 and 10 is consistent with elastic behavior ($\tan(\delta) < 0.5$). Q at pH 10 exhibits a lower $\tan(\delta)$, indicating more elastic behavior at pH 10 compared to 7.4. For Q at pH 6, the sample remains in the solution state (Fig. S3, ESI†).

While hydrophobic and ionic interactions are important for stabilizing coiled-coils, the overall charge of a protein can also modulate its assembly.[40] The electrostatic potential maps of Q protein from pH 4–12 reveal a significant change in charge distribution at pH 4 and at pH 11 and beyond (Fig. S4, ESI†). Despite exhibiting a similar profile as pH 7.4 and 10, Q at pH 6 did not result in gel formation. While protein aggregation is observed at pH 4, Q at pH 11 and 12 under different buffer conditions resulted in gelation at 4 °C (data not shown). To further explain this, we have calculated the overall charge of Q protein as a function of pH (Fig. 6 and Table S2, ESI†). Q exhibits a theoretical pI of 10.3 and maintains a net positive charge at $\leq$ pH 10. We posit that the electrostatic repulsions are predominant at the lower pH studied and reduces as the pH nears the isoelectric point, allowing the coiled-coils to stack and assemble into fibers, which are further entangled to form hydrogels. This is in agreement with the previous work on pH-responsive coiled-coil hydrogels by Fletcher *et al.*[9] Overall, Q undergoes faster gelation at a pH closer to pI. At charges $> +5$ for pH 6, the high net positive charge on the protein creates significant repulsion and prevents self-assembly. It is important

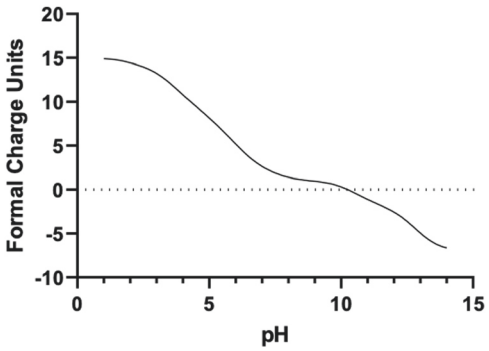


Fig. 6 Calculated net charge of Q protein as a function of pH.

to note that high salt concentrations may shield the Q surface and attenuate some of the long-range electrostatic effects due to charge as gelation does not take place in the absence of salt.

## Conclusions

In summary, self-assembly and gelation properties of an engineered protein are explored at three different pHs. At pH 6, due to electrostatic repulsions, Q forms nanoparticles that do not pack together to form a gel. At pH 7.4 and pH 10, Q self-assembles to form nanofibers that further assemble to form hydrogels. Consistent with the previous studies,[9] faster gelation of Q is observed at pH 10, which is closer to its isoelectric point. While Q at pH 6 is viscous, enhanced elastic properties are observed with increased pH for the range studied. We have previously characterized Q hydrogels at pH 8 for their thermoresponsiveness and ability to house and deliver small hydrophobic molecules.[21] Given the pH sensitivity of these hydrogels, they can serve as candidates to deliver chemotherapeutics, exploiting the acidic pH in tumors.[6,14,41] Overall, this study will potentially guide the development of novel scaffolds and functional biomaterials that are sensitive towards biologically relevant stimuli.

## Author contributions

All authors have given approval to the final version of the manuscript.

 

## Funding sources

This work was supported by NSF-DMREF under Award Number DMR 1728858, and NSF-MRSEC Program under Award Number DMR 1420073.

## Conflicts of interest

The authors declare no competing financial interest.

## Acknowledgements

The authors would like to acknowledge NYU Langone's Microscopy Laboratory. This shared resource is partially supported by the Cancer Center Support Grant P30CA016087 at the Laura and Isaac Perlmutter Cancer Center. We also thank Dr Jeffrey F. Morris and Nelya Akhmetkhanova for providing access to the rheometer at The City College of New York.

## References

1 P. Katyal, M. Meleties and J. K. Montclare, Self-Assembled Protein- and Peptide-Based Nanomaterials, *ACS Biomater. Sci. Eng.*, 2019, **5**(9), 4132–4147.
2 N. C. Abascal and L. Regan, The past, present and future of protein-based materials, *Open Biol.*, 2018, **8**, 10.
3 J. E. Gagner, W. Kim and E. L. Chaikof, Designing protein-based biomaterials for medical applications, *Acta Biomater.*, 2014, **10**(4), 1542–1557.
4 D. Sengupta and S. C. Heilshorn, Protein-Engineered Biomaterials: Highly Tunable Tissue Engineering Scaffolds, *Tissue Eng., Part B*, 2010, **16**(3), 285–293.
5 J. Kopecek and J. Yang, Smart self-assembled hybrid hydrogel biomaterials, *Angew. Chem., Int. Ed.*, 2012, **51**(30), 7396–7417.
6 P. Katyal, F. Mahmoudinobar and J. K. Montclare, Recent trends in peptide and protein-based hydrogels, *Curr. Opin. Struct. Biol.*, 2020, **63**, 97–105.
7 J. Kopeček, Hydrogel biomaterials: a smart future?, *Biomaterials*, 2007, **28**(34), 5185–5192.
8 P. S. Kowalski, C. Bhattacharya, S. Afewerki and R. Langer, Smart Biomaterials: Recent Advances and Future Directions, *ACS Biomater. Sci. Eng.*, 2018, **4**(11), 3809–3817.
9 N. L. Fletcher, C. V. Lockett and A. F. Dexter, A pH-responsive coiled-coil peptide hydrogel, *Soft Matter*, 2011, **7**(21), 10210–10218.
10 V. G. Phan, T. Thambi, B. S. Kim and D. S. Lee, Engineering highly swellable dual-responsive protein-based injectable hydrogels: the effects of molecular structure and composition *in vivo*, *Biomater. Sci.*, 2017, **5**(11), 2285–2294.
11 R. S. C. Su, Y. Kim and J. C. Liu, Resilin: protein-based elastomeric biomaterials, *Acta Biomater.*, 2014, **10**(4), 1601–1611.
12 R. Wang, Z. Yang, J. Luo, I.-M. Hsing and F. Sun, B12-dependent photoresponsive protein hydrogels for controlled stem cell/protein release, *Proc. Natl. Acad. Sci. U. S. A.*, 2017, **114**(23), 5912–5917.
13 A. Dasgupta, J. H. Mondal and D. Das, Peptide hydrogels, *RSC Adv.*, 2013, **3**(24), 9117–9149.
14 G. Ghosh, R. Barman, J. Sarkar and S. Ghosh, pH-Responsive Biocompatible Supramolecular Peptide Hydrogel. *The*, *J. Phys. Chem. B*, 2019, **123**(27), 5909–5915.
15 N. L. Goeden-Wood, J. D. Keasling and S. J. Muller, Self-assembly of a designed protein polymer into β-sheet fibrils and responsive gels, *Macromolecules*, 2003, **36**(8), 2932–2938.
16 D. J. Pochan, J. P. Schneider, J. Kretsinger, B. Ozbas, K. Rajagopal and L. Haines, Thermally reversible hydrogels via intramolecular folding and consequent self-assembly of a de novo designed peptide, *J. Am. Chem. Soc.*, 2003, **125**(39), 11802–11803.
17 H. Dong, S. E. Paramonov and J. D. Hartgerink, Self-Assembly of α-Helical Coiled Coil Nanofibers, *J. Am. Chem. Soc.*, 2008, **130**(41), 13691–13695.
18 W. A. Petka, J. L. Harden, K. P. McGrath, D. Wirtz and D. A. Tirrell, Reversible hydrogels from self-assembling artificial proteins, *Science*, 1998, **281**(5375), 389–392.
19 A. F. Dexter, N. L. Fletcher, R. G. Creasey, F. Filardo, M. W. Boehm and K. S. Jack, Fabrication and characterization of hydrogels formed from designer coiled-coil fibril-forming peptides, *RSC Adv.*, 2017, **7**(44), 27260–27271.
20 E. F. Banwell, E. S. Abelardo, D. J. Adams, M. A. Birchall, A. Corrigan, A. M. Donald, M. Kirkland, L. C. Serpell, M. F. Butler and D. N. Woolfson, Rational design and application of responsive alpha-helical peptide hydrogels, *Nat. Mater.*, 2009, **8**(7), 596–600.
21 L. K. Hill, M. Meleties, P. Katyal, X. Xie, E. Delgado-Fukushima, T. Jihad, C.-F. Liu, S. O'Neill, R. S. Tu, P. D. Renfrew, R. Bonneau, Y. Z. Wadghiri and J. K. Montclare, Thermoresponsive Protein-Engineered Coiled-Coil Hydrogel for Sustained Small Molecule Release, *Biomacromolecules*, 2019, **20**(9), 3340–3351.
22 J. Hume, J. Sun, R. Jacquet, P. D. Renfrew, J. A. Martin, R. Bonneau, M. L. Gilchrist and J. K. Montclare, Engineered coiled-coil protein microfibers, *Biomacromolecules*, 2014, **15**(10), 3503–3510.
23 A. S. Holehouse and R. V. Pappu, Encoding phase transitions, *Nat. Mater.*, 2015, **14**(11), 1083–1084.
24 E. Strable, D. E. Prasuhn, Jr., A. K. Udit, S. Brown, A. J. Link, J. T. Ngo, G. Lander, J. Quispe, C. S. Potter, B. Carragher, D. A. Tirrell and M. G. Finn, Unnatural amino acid incorporation into virus-like particles, *Bioconjugate Chem.*, 2008, **19**(4), 866–875.
25 P. Wang, W. Bohr, M. Otto, K. M. Danzer and B. Mizaikoff, Quantifying amyloid fibrils in protein mixtures *via* infrared attenuated-total-reflection spectroscopy, *Anal. Bioanal. Chem.*, 2015, **407**(14), 4015–4021.
26 X. Hu, D. Kaplan and P. Cebe, Determining Beta-Sheet Crystallinity in Fibrous Proteins by Thermal Analysis and Infrared Spectroscopy, *Macromolecules*, 2006, **39**(18), 6161–6170.
27 C. A. Schneider, W. S. Rasband and K. W. Eliceiri, NIH Image to ImageJ: 25 years of image analysis, *Nat. Methods*, 2012, **9**(7), 671–675.
28 W. D. Cornell, P. Cieplak, C. I. Bayly, I. R. Gould, K. M. Merz, D. M. Ferguson, D. C. Spellmeyer, T. Fox, J. W. Caldwell and P. A. Kollman, A second generation force field for the

simulation of proteins, nucleic acids, and organic molecules, *J. Am. Chem. Soc.*, 1995, **117**(19), 5179–5197.

29 D. C. Bas, D. M. Rogers and J. H. Jensen, Very fast prediction and rationalization of p$K_a$ values for protein–ligand complexes, *Proteins: Struct., Funct., Bioinf.*, 2008, **73**(3), 765–783.

30 H. Li, A. D. Robertson and J. H. Jensen, Very fast empirical prediction and rationalization of protein p$K_a$ values, *Proteins: Struct., Funct., Bioinf.*, 2005, **61**(4), 704–721.

31 R. Chari, K. Jerath, A. V. Badkar and D. S. Kalonia, Long- and Short-Range Electrostatic Interactions Affect the Rheology of Highly Concentrated Antibody Solutions, *Pharm. Res.*, 2009, **26**(12), 2607.

32 S. R. Raghavan and B. H. Cipriano, Gel Formation: Phase Diagrams Using Tabletop Rheology and Calorimetry, in *Molecular Gels: Materials with Self-Assembled Fibrillar Networks*, ed. R. G. Weiss and P. Terech, Springer Netherlands, Dordrecht, 2006, pp. 241–252.

33 S. K. Gunasekar, M. Asnani, C. Limbad, J. S. Haghpanah, W. Hom, H. Barra, S. Nanda, M. Lu and J. K. Montclare, N-terminal aliphatic residues dictate the structure, stability, assembly, and small molecule binding of the coiled-coil region of cartilage oligomeric matrix protein, *Biochemistry*, 2009, **48**(36), 8559–8567.

34 T. Heimburg, J. Schuenemann, K. Weber and N. Geisler, Specific recognition of coiled coils by infrared spectroscopy: analysis of the three structural domains of type III intermediate filament proteins, *Biochemistry*, 1996, **35**(5), 1375–1382.

35 T. Heimburg, J. Schunemann, K. Weber and N. Geisler, FTIR-Spectroscopy of multistranded coiled coil proteins, *Biochemistry*, 1999, **38**(39), 12727–12734.

36 M. Jackson and H. H. Mantsch, The use and misuse of FTIR spectroscopy in the determination of protein structure, *Crit. Rev. Biochem. Mol. Biol.*, 1995, **30**(2), 95–120.

37 M. O. Steinmetz, I. Jelesarov, W. M. Matousek, S. Honnappa, W. Jahnke, J. H. Missimer, S. Frank, A. T. Alexandrescu and R. A. Kammerer, Molecular basis of coiled-coil formation, *Proc. Natl. Acad. Sci. U. S. A.*, 2007, **104**(17), 7062–7067.

38 G. Indelicato, N. Wahome, P. Ringler, S. A. Muller, M. P. Nieh, P. Burkhard and R. Twarock, Principles Governing the Self-Assembly of Coiled-Coil Protein Nanoparticles, *Biophys. J.*, 2016, **110**(3), 646–660.

39 S. A. Potekhin, T. N. Melnik, V. Popov, N. F. Lanina, A. A. Vazina, P. Rigler, A. S. Verdini, G. Corradin and A. V. Kajava, *De novo* design of fibrils made of short α-helical coiled coil peptides, *Chem. Biol.*, 2001, **8**(11), 1025–1032.

40 P. Burkhard, J. Stetefeld and S. V. Strelkova, Coiled coils: a highly versatile protein folding motif, *Trends Cell Biol.*, 2001, **11**(2), 82–88.

41 A. I. Rezk, F. O. Obiweluozor, G. Choukrani, C. H. Park and C. S. Kim, Drug release and kinetic models of anticancer drug (BTZ) from a pH-responsive alginate polydopamine hydrogel: towards cancer chemotherapy, *Int. J. Biol. Macromol.*, 2019, **141**, 388–400.

 